Single-molecule characterization of a bright and photostable deep-red fluorescent squaraine-figure-eight (SF8) dye

Authors: Kirill Kniazev,^a † Tianle Guo,^a † Canjia Zhai,^a Rananjaya S. Gamage,^a Sushrut Ghonge^b, Pavel A. Frantsuzov^c, Masaru Kuno,^{a,b} Bradley Smith,^{a,*}

Affiliations:

^aDepartment of Chemistry and Biochemistry, University of Notre Dame, Notre Dame, IN 46556

^bDepartment of Physics, University of Notre Dame, Notre Dame, IN 46556

^cVoevodsky Institute of Chemical Kinetics and Combustion, Siberian Brunch of the Russian Academy of Science, Institutskaya 3, Novosibirsk, 630090, Russia

*Author to whom correspondence should be addressed: smith.115@nd.edu. Telephone: +1(574)6318632

†Contributed equally to this work.

ORCID ID Numbers

Kirill Kniazev: 0000-0002-7338-1436

Canjia Zhai: 0000-0002-5348-2790

Rananjaya S. Gamage: 0000-0003-3960-0276

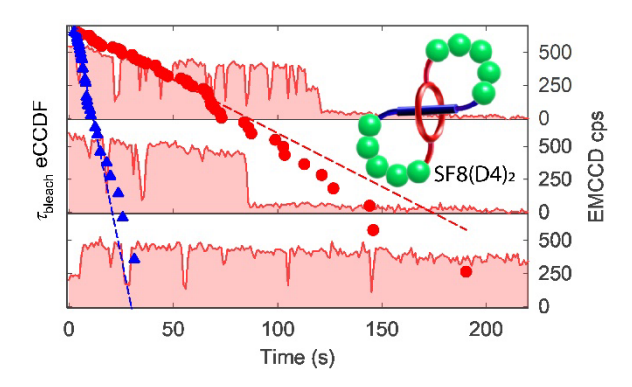
Sushrut Ghonge: 0000-0003-4370-3331

Pavel A. Frantsuzov: 0000-0002-7717-5453

Masaru Kuno: 0000-0003-4210-8514

Bradley Smith: 0000-0003-4120-3210

TOC Figure



Keywords: deep-red fluorescence, squaraine, single molecule, photostability, photon yield

Abstract:

Squaraine Figure Eight (SF8) dyes are a unique class of deep-red fluorescent dyes with self-threaded molecular architecture that provides structural rigidity while simultaneously encapsulating and protecting the emissive fluorochrome. Previous cell microscopy and bulk phase studies of SF8 dyes indicated order of magnitude enhancements in photostability over conventional pentamethine cyanine dyes such as Cy5. Studies conducted at the single molecule level now reveal that these ensemble level enhancements carry over to the single molecule level in terms of enhanced emission quantum yields, longer times to photobleaching, and enhanced total photon yields. When compared to Cy5, the SF8-based dye SF8(D4)₂ possesses a three-fold larger single molecule emission quantum yield, exhibits order of magnitude longer average times before photobleaching, and exhibits twenty times larger photon yields. Additional features such as water solubility, fluorochrome encapsulation to protect it against nucleophilic attack, and selective biomarker targeting capability make SF8-based dyes promising candidates for biological labeling and microscopy applications and single molecule tracking.

1. Introduction

The ongoing development of high-performance fluorescent dyes is driven by the increasing number of ways that microscopy and imaging are deployed within the life sciences.[1, 2, 3, 4, 5, 6, 7] In particular, many microscopy and imaging methods are more informative if they employ bright and durable fluorescent dyes with high photon outputs. Efforts to enhance dye fluorescent signals have led to modified experimental protocols that use chemical additives such as reducing agents or oxygen scavengers to increase the photostability and photon-count of a fluorescent dye during image acquisition.[8, 9, 10, 11] While this approach can be helpful in specific circumstances, incorporating added chemicals is potentially problematic

as it complicates experimental procedures and may induce undesired experimental artifacts. [12] The need for chemical additives is attenuated or perhaps even eliminated if a fluorescent dye possesses very high brightness and photochemical stability. This need is especially pressing for dyes that absorb and emit deepred or near-infrared light (wavelength >640 nm), wavelengths known to penetrate more deeply through opaque media and undergo less scattering. [12, 13] Unfortunately, extended chemical chromophores with conjugated π -electrons and small HOMO-LUMO energy difference - properties inherent to long wavelength organic dyes - are chemically reactive and often quite hydrophobic. The rational design of bright and stable, long wavelength organic fluorescent dyes thus represents a challenging problem in fluorescent molecular probe design, given the simultaneous need to satisfy multiple spectral, physical, and chemical criteria. [13, 14, 15]

Squaraine dyes were discovered in the 1960's and have been investigated extensively for many applications in different technical fields such as coatings, visual media, and biomedicine. [16] Squaraines exhibit narrow and intense deep-red absorption/fluorescence bands along with high emission quantum yields (QYs) in organic solvents. The photophysics of squaraine dyes in bulk solution have been extensively investigated.[17, 18, 19] One drawback that has diminished their impact in biomedical technology is the propensity of many squaraine dyes to degrade in the presence of nucleophiles. [20] In 2005, we showed how squaraine dyes could be synthetically encapsulated inside tetralactam macrocycles to produce squaraine rotaxanes.[21, 22] The steric protection provided by the encapsulation greatly enhances the squaraine chemical stability and also improves squaraine fluorescence brightness in biological media. Squaraine rotaxanes have near identical spectral properties as the pentamethine cyanine dye, Cy5, a standard benchmark fluorophore often used for deep-red fluorescence imaging and microscopy. Several direct comparisons have consistently shown that squaraine rotaxanes are more photostable than Cy5 and perform better as fluorescent molecular probes in cell microscopy experiments that require high levels of photoresistance. [23, 24, 25, 26] Of particular note is the emerging use of conjugatable squaraine rotaxane dyes as bright and long-lived fluorescent labels for informative antibody single molecule tracking studies.[27, 28, 29, 30, 31, 32, 33, 34] The commercial availability of squaraine rotaxane dyes has also enabled single molecule studies of fundamental photophysical phenomena such as fluorescence blinking[35] and switching.[36]

The increased utilization of squaraine rotaxanes for single molecule imaging has prompted us to pursue structural variations that have similarly high photophysical performance but with alternative biological targeting mechanisms. Our prior work has revealed that squaraine rotaxanes undergo a set of related intramolecular motions such as rotaxane shuttling or pirouetting.[22] This dynamic behavior could limit performance as a fluorescent molecular probe by providing a potential excited state relaxation pathway

that can diminish fluorescence brightness.[37, 38, 39] To decrease structural flexibility, we have developed a synthetic method that covalently connects the two interlocked components of a squaraine rotaxane to create a single, rigidified molecule with a self-threaded architecture and topology reminiscent of a molecular eight.[40] Moreover, we have recently reported a series of Squaraine Figure Eight (SF8) structures with two peptidyl loops and shown that they exhibit outstanding performance in different types of cell microscopy and in vivo imaging experiments. Notably, the conformationally constrained peptidyl loops within SF8 dyes provide superior fluorescent probe targeting properties compared to homologous squaraine rotaxanes with the same peptidyl sequence. Moreover, cell microscopy studies have demonstrated that the SF8 peptidyl sequence can be optimized to produce selective affinity for specific cell types (e.g., cancer cells that overexpress integrin receptors)[41] or specific organelles with cells (e.g., mitochondria).[42]

The focus of this present study is SF8(D4)₂ a water-soluble SF8-based dye with four aspartate residues within each identical peptidyl loop (**Scheme 1**). Previous studies have revealed that SF8(D4)₂ is unusually stable in two ways; (a) the surrounding macrocyclic component (colored red) sterically protects the encapsulated squaraine fluorochrome (colored blue) and blocks chemical attack of the dye by nucleophiles, and (b) the constrained peptidyl loops (colored green) resist degradation by protease enzymes compared to a homologous squaraine rotaxane with the same peptidyl sequence.[40] The polyanionic charge of SF8(D4)₂ prevents cell permeation, but the tetra-aspartate loops promote selective targeting to the mineral matrix within bone tissue, enabling selective fluorescence imaging of bone in complex biological media, including histology sections and living mice.[40]

The high promise of these fluorescence cell microscopy and in vivo imaging results has prompted us to conduct additional experiments that compare the photophysical properties of SF8(D4)₂ to Cy5 with an emphasis on factors that determine their performance in single molecule tracking experiments. The most important of these properties are fluorescence brightness (i.e. emission quantum yield), dye lifetime before photobleaching, and total photon yield for a single molecule. It is important to emphasize that all measurements in this study were made under ambient laboratory atmosphere with no attempt to enhance fluorescence properties by using chemical additives.

Scheme 1. Structures of the deep-red fluorescent dyes, SF8(D4)₂ and Cy5.

2. Results and Discussion

Spectra in **Figure 1** show that SF8(D4)₂ and Cy5 possess similar absorption and fluorescence maximum wavelengths and associated peak widths. At low micromolar concentration in water, both dyes disperse as monomeric species. We observe no evidence of static quenching due to dye self-association.[43] Listed in **Table 1** are peak molar extinction coefficients (ε_{peak}), molar extinction coefficients at 641 nm (ε_{641} nm), corresponding absorption cross sections at 641 nm (σ_{641} nm), excited state lifetimes (τ) (**Figure S1**), and fluorescence QYs (ϕ_f) in H₂O and D₂O. The latter have been measured using methylene blue as a QY reference.

Comparison of measured cross sections reveals that both dyes possess near identical photophysical responses at the ensemble level. Molar extinction coefficients and absorption cross sections differ by ~20-30%. Cy5's quantum yield in H_2O (20 ± 2 %), however, is lower than its value in D_2O (27 ± 2 %) by an amount consistent with literature reports.[12, 44, 45] In contrast, SF8(D4)₂'s QY in H_2O (19 ± 2 %) is statistically identical to that in D_2O (17 ± 2 %). The absence of a "heavy water effect" is due to spatial isolation of the encapsulated squaraine fluorochrome within SF8(D4)₂, which diminishes excited state deactivation by the surrounding hydration shell. More specifically, steric protection of the encapsulated squaraine reduces the likelihood of hydrogen-bond-assisted relaxation. Encapsulation also attenuates

quenching caused by dipole-dipole resonant energy transfer whose efficiency decays as the sixth power of the donor/acceptor distance.[46, 47]

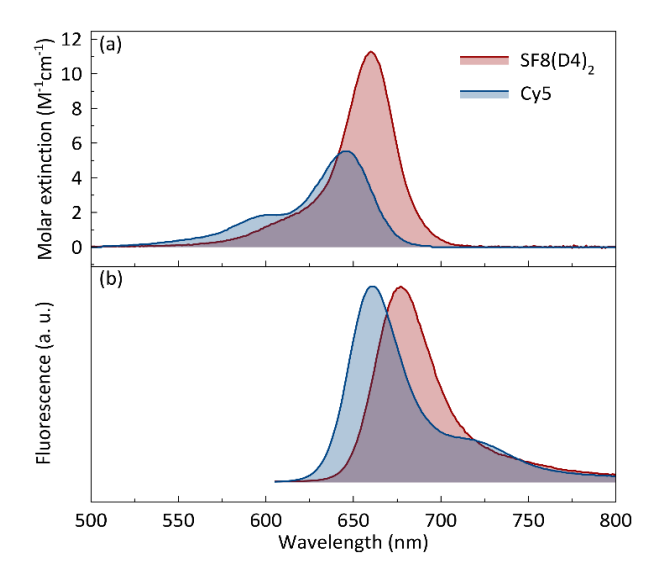


Figure 1. Molar extinction (a) and fluorescence (b) spectra of SF8(D4)₂ and Cy5 in H₂O. Emission spectra acquired by exciting specimens at 595 nm.

Table 1. Spectral properties of SF8(D4)₂ and Cy5.

	$\lambda_{abs} (nm)$	$\lambda_{em} \left(nm \right)$	$Log\epsilon_{peak}$	Log <i>€</i> _{641,nm}	$\sigma_{641 \text{ nm}} (\text{cm}^2)$	$\tau(ns)$	$\phi_{\rm f}$ (H ₂ O) b	$\phi_{\mathrm{f}}(\mathrm{D_2O})^b$
Dye	(FWHM) ^a	(FWHM) a						
SF8(D4) ₂	660 (40)	677 (34)	5.44	5.23	6.5×10 ⁻¹⁶	1.60	19 ± 2 %	17 ± 2 %
Cy5	646 (40)	664 (38)	5.32	5.29	7.5×10 ⁻¹⁶	0.77	$20\pm2~\%$	$27\pm2~\%$

^a FWHM is full width at half maximum.

Prior work has shown that a solution of SF8(D4)₂ is approximately ten times more photostable than an equivalent solution of Cy5.[40] There is good evidence that photobleaching of squaraine and cyanine dyes is predominantly due to dye reaction with photogenerated singlet oxygen.[48, 49] In principle, two independent factors determine dye photostability in an air-saturated solvent. One is the quantum yield for oxygen photosensitization. The other is the dye's reactivity with singlet oxygen. To elucidate the primary reason for the enhanced photostability of SF8(D4)₂ compared to Cy5, we measured each dye's relative quantum yield for oxygen photosensitization by conducting a series of classic singlet oxygen trapping experiments.[49, 50] These experiments entail irradiating separate aqueous solutions with broadband light, filtered to allow wavelengths > 520 nm. Each solution contains a binary mixture of deep-red dye and an

^b ϕ_f is fluorescence quantum yield relative to methylene blue in water ($\phi_f = 0.02$) at room temperature.

excess of 1,3-diphenylisobenzofuran (DPBF). DPBF absorbs at 415 nm and is not excited by the incident light. However, it reacts with singlet oxygen (photogenerated by the deep-red dye) to produce a bleached product. Initial rates of DPBF consumption, shown in **Figures 2a** and **2b**, are proportional to the photogenerated singlet oxygen concentration and indicate relative dye quantum yields for oxygen photosensitization.[50]

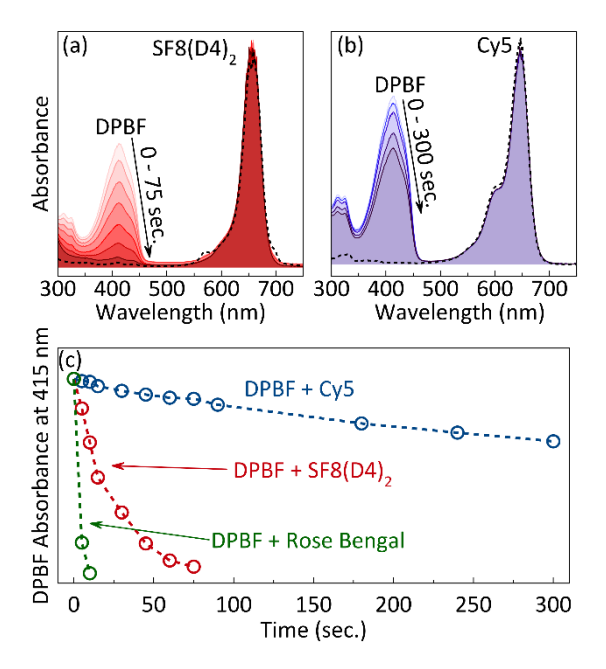


Figure 2. Change in normalized absorption spectra during broadband lamp irradiation ($\lambda > 520$ nm) at room temperature and exposed to air for separate solutions (THF:water, 1:4) that contain a binary mixture of (a) DPBF (75 μ M) and SF₈(D4)₂ (6 μ M), or (b) DPBF (75 μ M) and Cy5 (6 μ M). (c) Plots of decrease in DPBF absorbance at 415 nm over time due to DPBF reaction with photogenerated singlet oxygen.

Plots of DPBF consumption in **Figure 2c** show that an aqueous solution of SF8(D4)₂ photogenerates a ten times higher singlet oxygen flux than Cy5 under the same irradiation conditions. SF8(D4)₂ possesses an oxygen photosensitization efficiency comparable to a non-encapsulated squaraine dye[51, 52] and both are lower than that of the benchmark photosensitizer Rose Bengal (**Figure 2c**). Of note is that the data in **Figures 2a** and **2b** confirm that photobleaching of SF8(D4)₂ and Cy5 is primarily due to dye reaction with singlet oxygen. In both cases, there is negligible dye photobleaching because added DPBF acts as singlet oxygen scavenger to protect the two from photobleaching.[51, 52]

Even though SF8(D4)₂ photogenerates ten times more singlet oxygen than Cy5, the previously measured rate of SF8(D4)₂ photobleaching in bulk-solution is about ten times slower than Cy5.[40] There are two major reasons for this dramatic difference in dye reactivity. One is the difference in π -electron energy states; π -electrons in SF8(D4)₂ occupy relatively low energy aromatic orbitals and are less reactive

with electrophilic singlet oxygen than Cy5's π -electrons, which occupy relatively high energy polymethine orbitals. A second reason is the steric protection provided by SF8(D4)₂; that is, encapsulation of the squaraine's strained and relatively reactive C₄O₂ cyclic core inhibits any putative bimolecular reaction with singlet oxygen.

Next, we compare the photophysical properties of SF8(D4)₂ and Cy5 at the single-molecule level using widefield microscopy. A 641 nm continuous wave (CW) laser was used as the excitation source with laser light guided to the specimen through an inverted microscope (**Scheme S1**, Supplementary Data, **SD**). Widefield illumination was achieved by focusing the excitation onto the back focal plane of a 100x, 1.45 Numerical Aperture (NA) oil immersion objective to obtain a $\sim 50 \times 50 \, \mu \text{m}^2$ widefield excitation area. Samples consisted of separate solutions of SF8(D4)₂ or Cy5, diluted to a concentration of 100 nM in deionized water and spin-coated onto cleaned coverslips at 2000 RPM for 60 seconds. CW excitation intensities (I_{exc}) ranged from I_{exc} =20-200 W cm⁻² with resulting emission collected through the same objective using an electron-multiplying charge-coupled device (EMCCD) camera. See Experimental for more details

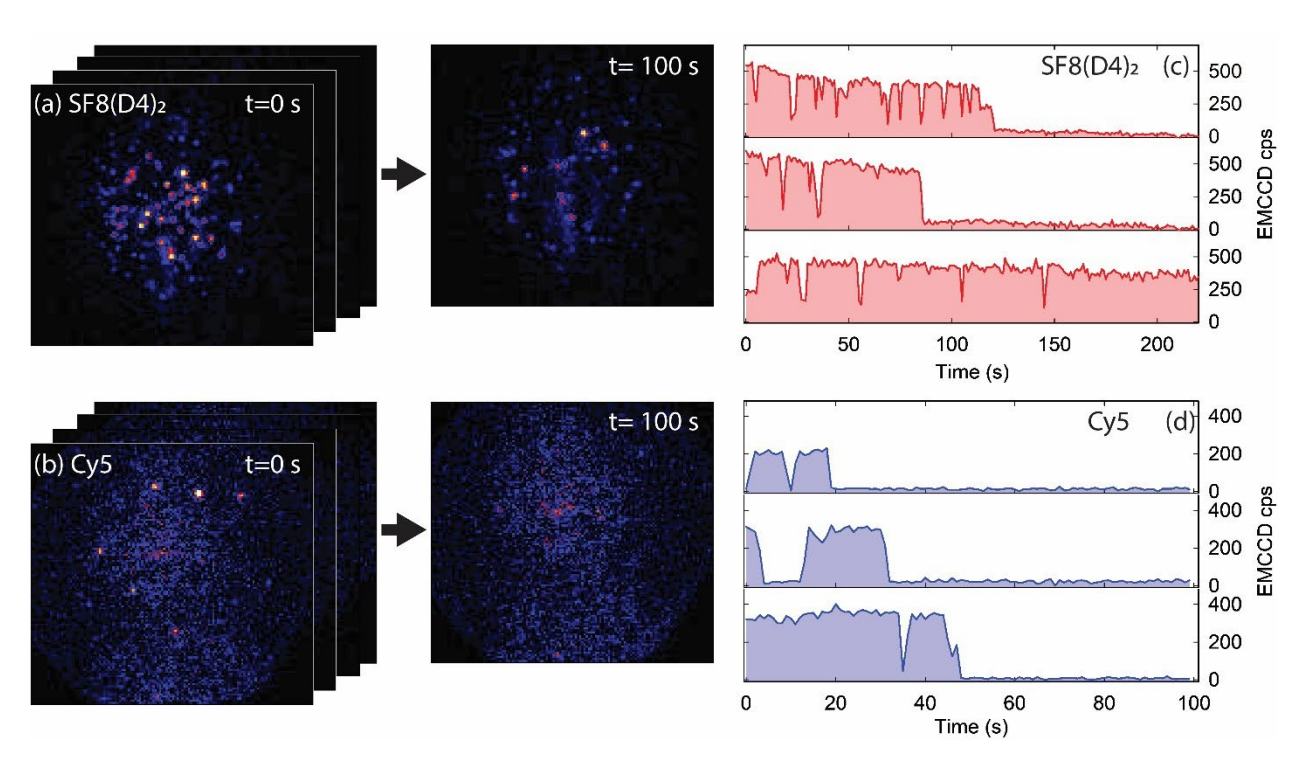


Figure 3. Single-molecule fluorescence images of spin-coated samples of (a) SF8(D4)₂ or (b) Cy5 (I_{exc} =200 W cm⁻²) acquired at the outset and after 100 seconds of CW 641 nm irradiation. (c,d) Representative 1 second integration I_{em} trajectories of individual (c) SF8(D4)₂ or (d) Cy5 molecules.

Figures 3a and 3b show two representative frames from separate SF8(D4)₂ and Cy5 fluorescence movies acquired at $I_{\rm exc}$ =200 W cm⁻². Complete video files have been provided as **Supplementary Data**. A visual comparison of images reveals SF8(D4)₂ to be brighter than the Cy5 and less photobleached after 100 seconds of continuous irradiation. More quantitative comparisons are possible by extracting the emission intensities of individual molecules in the acquired movies. **Figures 3c** and **3d** show representative $I_{\rm exc}$ =200 W cm⁻² SF8(D4)₂ and Cy5 emission intensity ($I_{\rm em}$) trajectories. All exhibit emissive "on" periods with intermittent intensity fluctuations that go beyond shot noise and that are characteristic of fluorescence intermittency.[53, 54] All trajectories end with single-step drops in brightness (i.e., complete disappearance of fluorescence), indicating single molecule photobleaching. **Figure S2** shows representative single molecule SF8(D4)₂ $I_{\rm em}$ trajectories acquired at other $I_{\rm exc}$ -values.

Average SF8(D4)₂ and Cy5 emission rates ($\langle I_{em} \rangle$) during I_{exc} =200 W cm⁻² trajectory "on" periods are $\langle I_{em} \rangle_{SF8(D4)_2}$ = 664 ± 418 cps and $\langle I_{em} \rangle_{Cy5}$ = 212 ± 146 cps. **Figure S3** shows that SF8(D4)₂ $\langle I_{em} \rangle_{cy5}$ values scale linearly with I_{exc} and suggests that employed excitation intensities are in the linear regime. Based on the photophysical parameters summarized in **Table 1**, corresponding SF8(D4)₂ and Cy5 saturation intensities ($I_{sat} = \frac{hv_{641\,\text{nm}}}{2\sigma_{641\,\text{nm}}\tau}$)[55] in a two-level system limit are $I_{sat}\sim$ 150 kW cm⁻² and $I_{sat}\sim$ 270 kW cm⁻², respectively. Different $I_{sat}\sim$ values predominantly originate from Cy5's shorter excited state lifetime.

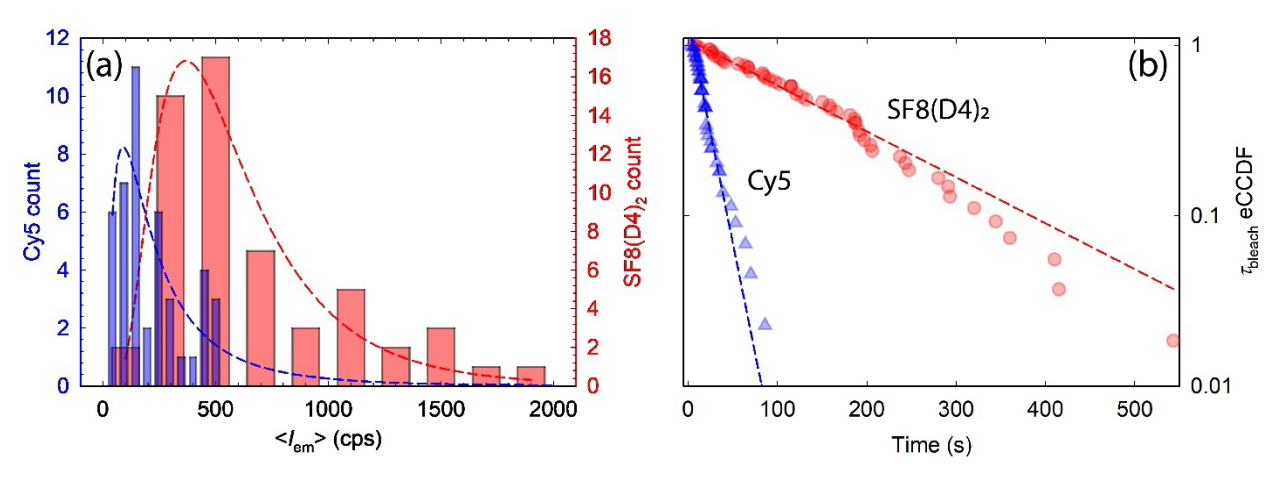


Figure 4. (a) Histograms of measured average SF8(D4)₂ and Cy5 single molecule $<I_{em}>$ -values during emissive periods of trajectories. Dashed lines are long-normal fits to the data. (b) SF8(D4)₂ and Cy5 τ_{bleach} eCCDF functions at I_{exc} =200 W cm⁻². Dashed lines are exponential decay fits with corresponding SF8(D4)₂ and Cy5 time constants of $<\tau_{bleach}>\sim$ 161 seconds and $<\tau_{bleach}>\sim$ 17 seconds, respectively.

The data make evident that SF8(D4)₂ is brighter than Cy5, a conclusion made more quantitative by generating histograms of observed $\langle I_{em} \rangle$ -values. **Figure 4a** summarizes resulting single molecule SF8(D4)₂ and Cy5 $\langle I_{em} \rangle$ histograms, which are related to corresponding emission QY distributions. Histograms can

be fit with log-normal functions (dashed red and blue lines) to obtain corresponding QY probability densities, i.e. $p_{\rm QY}({\rm QY}) = \frac{1}{{\rm QY}\sigma\sqrt{2\pi}}\exp\left(-\frac{(\ln{\rm QY}-\mu)^2}{2\sigma^2}\right)$ with μ the mean value of $\ln{\rm QY}$ and σ a standard deviation.

Distributed QYs point to a heterogeneity of local environments at the single molecule level that alter the efficiency of non-radiative relaxation following excitation. Offset SF8(D4)₂ and Cy5 distributions indicate that they possess different emission QYs at the single molecule level with SF8(D4)₂ being approximately three times brighter than Cy5. Offset distributions further suggest that Cy5's emission QYs are suppressed when immobilized onto substrates. This stems from near identical (starting) emission QYs between dyes reported in **Table 1**. We speculate that QY suppression originates from Cy5's chromophore being exposed to local environmental effects. In contrast, SF8(D4)₂'s squaraine fluorochrome is encapsulated and protected. The data thus suggest SF8(D4)₂ is intrinsically brighter than Cy5 and less prone to environmental perturbations when studied at the single molecule level.

Obtained emission trajectories simultaneously point to SF8(D4)₂ as significantly more robust to irreversible photobleaching than Cy5. Enhanced photostability can be quantified by extracting photobleaching lifetimes (τ_{bleach}) from individual SF8(D4)₂ and Cy5 single molecule trajectories using an unsupervised Hidden Markov Model (HMM) with combined Silhouette analysis.[56] Resulting τ_{bleach} histograms at a given I_{exc} are then converted into empirical Complementary Cumulative Distribution Functions (eCCDFs)[57] via

$$eCCDF(t) = \frac{1}{N} \sum_{i=1}^{N} \theta \left(\tau_{\text{bleach},i} - t \right)$$
 (1)

where N is the total single molecule trajectory sample size and $\theta(\tau_{\mathrm{bleach},i}-t)$ is the Heavyside function. Resulting functions, plotted in **Figure 4b**, reflect survival probabilities for unwanted dye photochemistry. They show exponential SF8(D4)₂ and Cy5 eCCDFs from where linear fits on a semilogarithmic scale yield 1/e (average) decay constants ($<\tau_{\mathrm{bleach}}>$) that represent characteristic photobleaching lifetimes for a given I_{exc} . Resulting $<\tau_{\mathrm{bleach}}>$ -values for SF8(D4)₂ and Cy5 at $I_{\mathrm{exc}}=200~\mathrm{W}~\mathrm{cm}^{-2}$ are $<\tau_{\mathrm{bleach},\mathrm{SF8(D4)_2}}>$ -161 seconds and $<\tau_{\mathrm{bleach},\mathrm{Cy5}}>$ -17 seconds. This illustrates an order of magnitude (temporal) difference in SF8(D4)₂ photochemical robustness. **Figure S4** provides visual details of the above eCCDF analysis. From this, we establish that observed photobleaching chemistries follow first order kinetics with associated photobleaching probability densities that are exponentially distributed, i.e. $p_{\mathrm{bleach}}(t) = \frac{1}{(\tau_{\mathrm{bleach}})}e^{-\frac{t}{(\tau_{\mathrm{bleach}})}}$.

Figures 5a and **5b** show single molecule $\langle I_{em} \rangle$ and τ_{bleach} correlation plots for SF8(D4)₂ or Cy5. Each point on the plots reflects the emissive ($\langle I_{em} \rangle$ and τ_{bleach}) behavior of an individual single molecule SF8(D4)₂ or Cy5 fluorescence trajectory. The data reveal an empirical inverse relationship between these two photophysical parameters. This is evident from data clustering at the bottom right corner of the plots, accompanied by overall sparseness of very bright and very long-lived individual molecules. In short, most SF8(D4)₂ or Cy5 molecules are (relatively speaking) dim and short-lived.; few are bright and long-lived. We posit that this inverse relationship arises from the combined effects of abovementioned independent QY and τ_{bleach} distributions (**Figure 4**). What results is a statistical favoring of dim and short-lived molecules over corresponding bright and long-lived species.

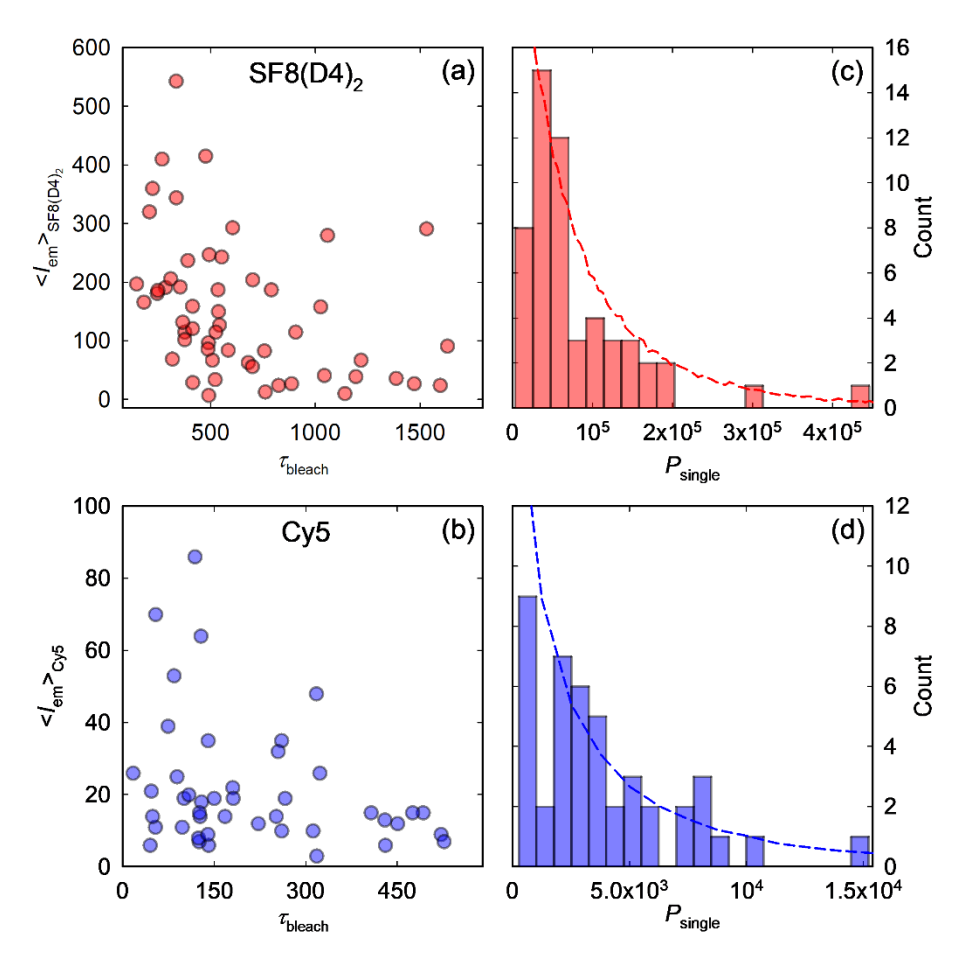


Figure 5. I_{exc} =200 W cm⁻² $< I_{\text{em}} >$ and τ_{bleach} correlation plot for (a) SF8(D4)₂ and (b) Cy5. Corresponding (c) SF8(D4)₂ and (d) Cy5 histograms of total, single molecule emitted photons prior to photobleaching. Dashed lines in (c) and (d) are numerical evaluations of **Equation 3**.

The observed inverse correlation is made more evident by plotting the total number of photons emitted by a single molecule before photobleaching (P_{single}). These are illustrated using histograms of

individual SF8(D4)₂ and Cy5 P_{single} -values in **Figures 5c** and **5d**. The data show that rather than exhibiting uniform or even peaked distributions, SF8(D4)₂ and Cy5 histograms fall off with increasing P_{single} -value.

Decaying P_{single} histograms can be rationalized since P_{single} is the product of individual, single molecule $\langle I_{\text{em}} \rangle$ and τ_{bleach} values, i.e.

$$P_{\text{single}} = G\eta \langle I_{\text{em}} \rangle \tau_{\text{bleach}} \tag{2}$$

where $G = \frac{I_{\rm exc}\sigma_{641\,nm}}{h\nu_{641\,nm}}$ is an excitation rate and η is an instrument photon collection efficiency. In practice, $P_{\rm single}$ arises from $\langle I_{\rm em} \rangle$ and $\tau_{\rm bleach}$ -values independently distributed in log-normal (**Figure 4a**) and exponentially decaying (**Figure 4b**) fashions. $P_{\rm single}$ therefore adopts distributed values obtained from the joint distribution function, $p(QY, t) = p_{QY}(QY)p_{\rm bleach}(t)$. A formal $P_{\rm single}$ probability distribution function is [58]

$$p(P_{\text{single}}) = \int_0^\infty p_{\text{QY}} \left(\frac{P_{\text{single}}}{Gnt}\right) p_{\text{bleach}}(t) \frac{1}{t} dt,$$
 (3)

which can be visualized using **Equation 2** along with I_{em} - and τ_{bleach} -values sampled from their respective $p_{QY}(QY)$ and $p_{bleach}(t)$ distributions. Dashed lines in **Figures 5c** and **5d** reveal that **Equation 3** indeed reproduces experimental SF8(D4)₂ and Cy5 P_{single} distributions. Qualitatively, the existence of independent QY and τ_{bleach} distributions suggests that complex environmental and chemical factors at the single molecule level dictate the photophysical performance of a given fluorescent dye. This further motivates efforts to create new dyes such as SF8(D4)₂ that encapsulate and isolate fluorochromes from environmental perturbations as well as chemical attack.

Average SF8(D4)₂ and Cy5 P_{single} -values are ~8×10⁴ and ~4×10³ observed EMCCD counts at I_{exc} =200 W cm⁻². This illustrates that SF8(D4)₂ is nearly twenty times more emissive in terms of photon yield than Cy5 under the same conditions. **Table 2** summarizes resulting SF8(D4)₂ P_{single} -values for all I_{exc} . Also included in **Table 2** are corresponding $< I_{\text{em}} >$ and $< \tau_{\text{bleach}} >$ values for all I_{exc} . In whole, the data confirm the enhanced robustness of SF8(D4)₂ over Cy5 in terms of single molecule QYs, dye photobleaching lifetimes, and photon yields.

Table 2. Summary of single molecule SF8(D4)₂ $< I_{cm} >$ -values, $< \tau_{bleach} >$ and P_{single} -values

I _{exc} (W cm ⁻²)	$< I_{em} > (cps)$	$<\tau_{\text{bleach}}>$ (s)	$P_{ m single}$
200	~645	~153	~8×10 ⁴
140	~282	~102	$\sim 3 \times 10^4$
30	~56	~88	$\sim 5 \times 10^3$
20	~46	~146	~6×10 ³

We were curious to rank the single molecule properties of SF8(D4)₂ relative to literature fluorescent dyes other than Cy5. Unfortunately, most reports on single molecule deep-red dyes do not provide enough experimental information to permit a meaningful comparison of measured values. We have identified two literature studies with sufficient experimental detail. One publication by Yang *et al.* evaluated a deep-red fluorescent BODIPY dye that is one of the brightest deep-red fluorophores ever reported.[59] They found that irradiating a sample of immobilized single dye molecules with no chemical additives at I_{exc} =130 W cm⁻² produced a measured photobleaching (1/e) lifetime of τ_{bleach} =3.3 ± 0.2 seconds. This value is approximately fifty times shorter than SF8(D4)₂'s $<\tau_{bleach}>\sim$ 161 seconds at I_{exc} =200 W cm⁻². Another publication by Tynan *et al.*,[60] characterized four different deep-red and near-infrared cyanine dyes and determined 1/e photobleaching lifetimes to be in the range of 2.2-7.1 seconds. This is about 30 percent of the value that we observe for Cy5, and 23 to 73 times shorter than the characteristic photobleaching lifetime for SF8(D4)₂ at I_{exc} =200 W cm⁻². Collectively, these comparisons highlight the remarkably high photostability of SF8(D4)₂ and its excellent suitability for incorporation into single molecule tracking experiments. More details about our literature analysis can be found in the **Supplementary Data**.

3. Conclusions

The deep-red fluorescent dye SF8(D4)₂ exhibits very high photostability at the single-molecule level. Compared to the benchmark pentamethine cyanine dye, Cy5, SF8(D4)₂ possesses a three-fold larger emission QY when immobilized at the single molecule level, exhibits a ~10 times longer average lifetime before photobleaching, and possesses a ~20 times larger total photon yield. As a new class of deep-red fluorophores, Squaraine Figure Eight (SF8) dyes are intrinsically bright and very stable; moreover, the peptidyl loops within the dye structures can be engineered to produce selective affinity for various types of

biomedically important targets.[40, 41, 42] SF8 dyes are thus likely to be especially useful for various photon-intensive microscopy, imaging, and diagnostics technologies.

4. Experimental

Materials

SF8(D4)₂ and Cy5 were prepared previously,[40] and the high purity for this study was confirmed by NMR spectroscopy. 1,3-Diphenylisobenzofuran was purchased from Sigma-Aldrich. Absorption spectra were collected on Evolution 201 UV/Vis Spectrometer with Thermo Insight software. Fluorescence spectra were collected using a Horiba Fluoromax4 Fluorometer with FluoroEssence software. Measurements were conducted at room temperature with quartz cuvettes (1 mL, 1 cm path length). Fluorescence lifetime data were acquired using a Horiba Fluorocube time correlated single photon counting system with a 560 nm NanoLED source (1 MHz repetition rate) and an IBH DataStation Hub for timing.

Measurement of Singlet Oxygen Photogeneration

An aliquot of DPBF (75 mM) was added to separate solutions of Cy5 (6 μ M) or SF8(D4)₂ (6 μ M) in THF-water (1:4) mixtures. Uncapped cuvette samples were irradiated using a 150 W tungsten lamp equipped with a 520 nm long pass filter to avoid direct excitation of DPBF. Absorption spectra were recorded at different time points up to 300 seconds.

Fluorescence Quantum Yield Measurements

Methylene blue ($\phi_f = 0.02$ in water) was employed as a reference standard with no attempt to exclude atmospheric oxygen.[40] Dye absorption for each sample in deionized H₂O or D₂O was adjusted to 0.08 at 600 nm to avoid the inner filter effect. A fluorescence spectrum of each dye solution was acquired (ex: 600 nm, slit width = 2 nm) and the integrated area used to calculate relative QYs.[40]

Single-Molecule Imaging and Photobleaching Lifetime Measurements

The single-molecule optical setup (**Scheme S1**) consisted of continuous wave excitation from a 641 nm laser (Coherent, OBIS). The laser output's linear polarization was converted to circular polarization using a quarter-wave plate (λ /4). Resulting circularly polarized light was then focused onto the back focal plane of a 100x, 1.45 NA oil immersion objective (Nikon) using a plan convex lens to obtain a ~ 50×50 μ m² widefield spot. A 650 nm long pass filter (Semrock) was used to reject any stray laser light. Filtered emission was detected using an electron multiplying charge camera device (Andor iXon 897). For either

SF8(D4)₂ or Cy5, integration times were 1 second. Single molecule $I_{\rm em}$ trajectories of emitting spots in EMCCD videos were extracted and analyzed using home-written Python code. Single molecules were identified based on IRAFStarFinder's algorithm using the astropy/photutils package[61], which calculates the target's centroid, roundness, and sharpness using image moments.

Acknowledgements

We are grateful for funding from the NIH (R35GM136212) as well as the Keck Foundation. MK thanks the National Science Foundation (CHE-1954724) for partial financial support of this study.

Notes

The authors declare no competing financial interest.

Supplementary Data

Scheme of the widefield single molecule imaging instrument, Single molecule SF8(D4)₂ and Cy5 video files, Representative single molecule SF8(D4)₂ I_{em} trajectories acquired at other I_{exc} -values, SF8(D4)₂ $< I_{em} >$ -values versus I_{exc} , Visual details of the τ_{bleach} eCCDF analysis, and Details about the literature analysis of τ_{bleach} for other dyes.

References

[1] Zhu H, Fan J, Du J, Peng X. Fluorescent probes for sensing and imaging within specific cellular organelles. Acc Chem Res 2016;49:2115–26. https://doi.org/10.1021/acs.accounts.6b00292.

[2] Klymchenko S, Solvatochromic A. Fluorogenic dyes as environment-sensitive probes: design and biological applications. Acc Chem Res 2017;50:366–75. https://doi.org/10.1021/acs.accounts.6b00517.

[3] Gao M, Yu F, Lv C, Choo J, Chen L. Fluorescent chemical probes for accurate tumor diagnosis and targeting therapy. Chem Soc Rev 2017;46:2237–71. https://doi.org/10.1039/C6CS00908E.

[4] Wang L, Du W, Hu Z, Uvdal K, Li L, Huang W. Hybrid rhodamine fluorophores in the visible/NIR region for biological imaging. Angew Chem Int Ed 2019;58:14026–43. https://doi.org/https://doi.org/10.1002/anie.201901061.

[5] Lu L, Wu Z, Li X, Han F. State-of-the-art: functional fluorescent probes for bioimaging and pharmacological research. Acta Pharmacol Sin 2019;40:717–23. https://doi.org/10.1038/s41401-018-0190-8.

- [6] Svechkarev D, Mohs AM. Organic fluorescent dye-based nanomaterials: advances in the rational design for imaging and sensing applications. Curr Med Chem 2019;26:4042–64. https://doi.org/10.2174/0929867325666180226111716.
- [7] Xiao D, Qi H, Teng Y, Pierre D, Kutoka PT, Liu D. Advances and challenges of fluorescent nanomaterials for synthesis and biomedical applications. Nanoscale Res Lett 2021;16:167. https://doi.org/10.1186/s11671-021-03613-z.
- [8] Zheng Q, Juette MF, Jockusch S, Wasserman MR, Zhou Z, Altman RB, et al. Ultra-stable organic fluorophores for single-molecule research. Chem Soc Rev 2014;43:1044–56. https://doi.org/10.1039/C3CS60237K.
- [9] Yang SK, Shi X, Park S, Ha T, Zimmerman SC. A dendritic single-molecule fluorescent probe that is monovalent, photostable and minimally blinking. Nat Chem 2013;5:692–7. https://doi.org/10.1038/nchem.1706.
- [10] Wu X, Zhu W. Stability enhancement of fluorophores for lighting up practical application in bioimaging. Chem Soc Rev 2015;44:4179–84. https://doi.org/10.1039/C4CS00152D.
- [11] Aitken CE, Marshall RA, Puglisi JD. An oxygen scavenging system for improvement of dye stability in single-molecule fluorescence experiments. Biophys J. 2008;94:1826–35. https://doi.org/10.1529/biophysj.107.117689
- [12] Klehs K, Spahn C, Endesfelder U, Lee SF, Fürstenberg A, Heilemann M. Increasing the brightness of cyanine fluorophores for single-molecule and superresolution imaging. Chem Phys Chem 2014;15:637–41. https://doi.org/10.1002/cphc.201300874.
- [13] Li J, Dong Y, Wei R, Jiang G, Yao C, Lv M, et al. Stable, bright, and long-fluorescence-lifetime dyes for deep-near-infrared bioimaging. J Am Chem Soc 2022;144:14351–62. https://doi.org/10.1021/jacs.2c05826.
- [14] Chen X, Zhang D, Su N, Bao B, Xie X, Zuo F, et al. Visualizing RNA dynamics in live cells with bright and stable fluorescent RNAs. Nat Biotechnol 2019;37:1287–93. https://doi.org/10.1038/s41587-019-0249-1.
- [15] Zhou L, Wang Q, Tan Y, Lang MJ, Sun H, Liu X. Rational development of near-infrared fluorophores with large stokes shifts, bright one-photon, and two-photon emissions for bioimaging and biosensing applications. Eur J Chem 2017;23:8736–40. https://doi.org/https://doi.org/10.1002/chem.201701365.
- [16] Xia G, Wang H. Squaraine dyes: the hierarchical synthesis and its application in optical detection. J Photochem Photobiol C 2017;31:84–113. https://doi.org/10.1016/j.jphotochemrev.2017.03.001.
- [17] Salice P, Arnbjerg J, Pedersen BW, Toftegaard R, Beverina L, Pagani GA, et al. Photophysics of squaraine dyes: role of charge-transfer in singlet oxygen production and removal. J Phys Chem A 2010;114:2518–25. https://doi.org/10.1021/jp911180n.
- [18] Tatarets AL, Fedyunyayeva IA, Dyubko TS, Povrozin YA, Doroshenko AO, Terpetschnig EA, et al. Synthesis of water-soluble, ring-substituted squaraine dyes and their evaluation as fluorescent probes and labels. Anal Chim Acta 2006;570:214–23. https://doi.org/10.1016/j.aca.2006.04.019.
- [19] Avirah RR, Jayaram DT, Adarsh N, Ramaiah D. Squaraine dyes in PDT: from basic design to in vivo demonstration. Org Biomol Chem 2012;10:911–20. https://doi.org/10.1039/c1ob06588b.

- [20] Ilina K, MacCuaig WM, Laramie M, Jeouty JN, McNally LR, Henary M. Squaraine Dyes: Molecular Design for Different Applications and Remaining Challenges. Bioconjug Chem 2020;31:194–213. https://doi.org/10.1021/acs.bioconjchem.9b00482.
- [21] Arunkumar E, Forbes CC, Noll BC, Smith BD. Squaraine-derived rotaxanes: sterically protected fluorescent near-IR dyes. J Am Chem Soc 2005;127:3288–9. https://doi.org/10.1021/ja042404n.
- [22] Gassensmith JJ, Baumes JM, Smith BD. Discovery and early development of squaraine rotaxanes. Chem Comms 2009;42:6329–38. https://doi.org/10.1039/b911064j.
- [23] Johnson JR, Fu N, Arunkumar E, Leevy WM, Gammon ST, Piwnica-Worms D, et al. Squaraine rotaxanes: superior substitutes for Cy-5 in molecular probes for near-infrared fluorescence cell imaging. Angew Chem Int Ed 2007;46:5528–31. https://doi.org/10.1002/anie.200701491.
- [24] Duggal D, Nagwekar J, Rich R, Midde K, Fudala R, Gryczynski I, et al. Phosphorylation of myosin regulatory light chain has minimal effect on kinetics and distribution of orientations of cross bridges of rabbit skeletal muscle. Am J Physiol Regul 2013;306:R222–33. https://doi.org/10.1152/ajpregu.00382.2013.
- [25] Adablah JE, Wang Y, Donohue M, Roper MG. Profiling glucose-stimulated and m3 receptor-activated insulin secretion dynamics from islets of 3angerhans using an extended-lifetime fluorescence dye. Anal Chem 2020;92:8464–71. https://doi.org/10.1021/acs.analchem.0c01226.
- [26] Patsenker LD, Tatarets AL, Povrozin YA, Terpetschnig EA. Long-wavelength fluorescence lifetime labels. Bioanal Rev 2011;3:115–37. https://doi.org/10.1007/s12566-011-0025-2.
- [27] Tsunoyama TA, Watanabe Y, Goto J, Naito K, Kasai RS, Suzuki KGN, et al. Super-long single-molecule tracking reveals dynamic-anchorage-induced integrin function. Nat Chem Biol 2018;14:497–506. https://doi.org/10.1038/s41589-018-0032-5.
- [28] Schlegel J, Peters S, Doose S, Schubert-Unkmeir A, Sauer M. Super-resolution microscopy reveals local accumulation of plasma membrane gangliosides at neisseria meningitidis invasion sites. Front Cell Dev Biol 2019;7:124. https://doi.org/10.3389/fcell.2019.00194.
- [29] Wäldchen F, Schlegel J, Götz R, Luciano M, Schnermann M, Doose S, et al. Whole-cell imaging of plasma membrane receptors by 3D lattice light-sheet dSTORM. Nat Commun 2020;11:1–6. https://doi.org/10.1038/s41467-020-14731-0.
- [30] Ojima K, Shiraiwa K, Soga K, Doura T, Takato M, Komatsu K, et al. Ligand-directed two-step labeling to quantify neuronal glutamate receptor trafficking. Nat Commun 2021;12:831. https://doi.org/10.1038/s41467-021-21082-x.
- [31] Shirai YM, Tsunoyama TA, Hiramoto-Yamaki N, Hirosawa KM, Shibata ACE, Kondo K, et al. Cortical actin nodes: their dynamics and recruitment of podosomal proteins as revealed by super-resolution and single-molecule microscopy. PLoS One 2017;12:1–26. https://doi.org/10.1371/journal.pone.0188778.
- [32] Flach A-C, Litke T, Strauss J, Haberl M, Gómez CC, Reindl M, et al. Autoantibody-boosted T-cell reactivation in the target organ triggers manifestation of autoimmune CNS disease. Proc Natl Acad Sci U S A 2016;113:3323–8. https://doi.org/10.1073/pnas.1519608113.
- [33] Perez Bay AE, Schreiner R, Benedicto I, Rodriguez-Boulan EJ. Galectin-4-mediated transcytosis of transferrin receptor. J Cell Sci 2014;127:4457–69. https://doi.org/10.1242/jcs.153437.

- [34] Perez Bay AE, Schreiner R, Benedicto I, Paz Marzolo M, Banfelder J, Weinstein AM, et al. The fast-recycling receptor Megalin defines the apical recycling pathway of epithelial cells. Nat Commun 2016;7:1–15. https://doi.org/10.1038/ncomms11550.
- [35] Wu R, Chen R, Zhou H, Qin Y, Zhang G, Qin C, et al. Detection of ultra-low oxygen concentration based on the fluorescence blinking dynamics of single molecules. Appl Phys Lett 2018;112:1–6. https://doi.org/10.1063/1.5005157.
- [36] Wu R, Chen R, Qin C, Gao Y, Qiao Z, Zhang G, et al. An electric field induced reversible single-molecule fluorescence switch. Chem Comms 2015;51:7368–71. https://dosi.org/10.1039/C5CC00850F.
- [37] Cao M, Zhu T, Zhao M, Meng F, Liu Z, Wang J, et al. Structure Rigidification Promoted Ultrabright Solvatochromic Fluorescent Probes for Super-Resolution Imaging of Cytosolic and Nuclear Lipid Droplets. Anal Chem 2022;94:10676–84. https://doi.org/10.1021/acs.analchem.2c00964.
- [38] Kreß KC, Bader K, Stumpe J, Eichhorn SH, Laschat S, Fischer T. Rigidified merocyanine dyes with different aspect ratios: dichroism and photostability. Dyes Pigm 2015;121:46–56. https://doi.org/https://doi.org/10.1016/j.dyepig.2015.04.041.
- [39] Michie MS, Götz R, Franke C, Bowler M, Kumari N, Magidson V, et al. Cyanine conformational restraint in the far-red range. J Am Chem Soc 2017;139:12406–9. https://doi.org/10.1021/jacs.7b07272.
- [40] Zhai C, Schreiber CL, Padilla-Coley S, Oliver AG, Smith BD. Fluorescent self-threaded peptide probes for biological imaging. Angew Chem Int Ed 2020;59:23740–7. https://doi.org/10.1002/anie.202009599.
- [41] Schreiber CL, Zhai C, Smith BD. Structural engineering of fluorescent self-threaded peptide probes for targeted cell imaging. Photochem Photobiol 2022;98:354–61. https://doi.org/10.1111/php.13439.
- [42] Schreiber CL, Zhai C, Smith BD. Chiral figure-eight molecular scaffold for fluorescent probe development. Org Biomol Chem 2021;19:3213–9. https://doi.org/10.1039/d1ob00306b.
- [43] Fürstenberg A. Water in biomolecular fluorescence spectroscopy and imaging: side effects and remedies. Chimia (Aarau) 2017;71:26–31. https://doi.org/10.2533/chimia.2017.26.
- [44] Kučera J, Peš O, Janovič T, Hofr C, Kubinyiová L, Tóth J, et al. Enhancement of luminescence signal by deuterated water practical implications. Sens Actuators B Chem 2022;352:131029. https://doi.org/10.1016/j.snb.2021.131029.
- [45] Maillard J, Klehs K, Rumble C, Vauthey E, Heilemann M, Fürstenberg A. Universal quenching of common fluorescent probes by water and alcohols. Chem Sci 2021;12:1352–62. https://doi.org/10.1039/d0sc05431c.
- [46] Das S, Thomas KG, Ramanathan R, George M V. Photochemistry of squaraine dyes. 6. Solvent hydrogen bonding effects on the photophysical properties of bis(benzothiazolylidene)squaraines. J Phys Chem 1993;97:13625–8. https://doi.org/10.1021/j100153a033.
- [47] Law KY. Squaraine chemistry. A study of the solute-solvent complexation of squaraine in solvents by proton NMR spectroscopy. J Phys Chem 1989;93:5925–30. https://doi.org/10.1021/j100352a054.
- [48] Nani RR, Kelley JA, Ivanic J, Schnermann MJ. Reactive species involved in the regioselective photooxidation of heptamethine cyanines. Chem Sci 2015;6:6556–63. https://doi.org/10.1039/c5sc02396c.

- [49] Friães S, Lima E, Boto RE, Ferreira D, Fernandes JR, Ferreira LFV, et al. Photophysicochemical properties and in vitro phototherapeutic effects of iodoquinoline- and benzothiazole-derived unsymmetrical squaraine cyanine dyes. Applied Sciences 2019;9:5414. https://doi.org/10.3390/app9245414.
- [50] Usui Y, Kamogawa K. A standard system to determine the quantum yield of singlet oxygen formation in aqueous solution. Photochem Photobiol 1974;19:245–7. https://doi.org/https://doi.org/10.1111/j.1751-1097.1974.tb06506.x.
- [51] Arunkumar E, Sudeep PK, Kamat P V., Noll BC, Smith BD. Singlet oxygen generation using iodinated squaraine and squaraine-rotaxane dyes. New J Chem 2007;31:677–83. https://doi.org/10.1039/b616224j.
- [52] Beverina L, Abbotto A, Landenna M, Cerminara M, Tubino R, Meinardi F, et al. New π -extended water-soluble squaraines as singlet oxygen generators. Org Lett 2005;7:4257–60. https://doi.org/10.1021/ol0516871.
- [53] P. J. Krüger T, Ilioaia C, van Grondelle R. Fluorescence Intermittency from the Main Plant Light-Harvesting Complex: Resolving Shifts between Intensity Levels. J Phys Chem B 2011;115:5071–82. https://doi.org/10.1021/jp201609c.
- [54] Ruth A, Hayashi M, Zapol P, Si J, McDonald MP, Morozov Y v, et al. Fluorescence intermittency originates from reclustering in two-dimensional organic semiconductors. Nat Commun 2017;8:14521. https://doi.org/10.1038/ncomms14521.
- [55] Moerner WE, Fromm DP. Methods of single-molecule fluorescence spectroscopy and microscopy. Rev Sci Instrum 2003;74:3597–619. https://doi.org/10.1063/1.1589587.
- [56] Pedregosa F, Varoquaux G, Gramfort A, Michel V, Thirion B, et al. Scikit-learn: Machine Learning in Python. J Mach Learn Res 2011;12:2825–2830. https://doi.org/10.5555/1953048.2078195.
- [57] Sornette Didier. critical phenomena in natural sciences: chaos, fractals, self-organization and disorder: concepts and tools. Heidelberg: Springer Series in Synergetics; 2006.
- [58] Springer M. D. The algebra of random variables. New York: Wiley; 1979.
- [59] Yang SK, Shi X, Park S, Ha T, Zimmerman SC. A dendritic single-molecule fluorescent probe that is monovalent, photostable and minimally blinking. Nat Chem 2013;5:692–7. https://doi.org/10.1038/nchem.1706.
- [60] Tynan CJ, Clarke DT, Coles BC, Rolfe DJ, Martin-Fernandez ML, Webb SED. Multicolour Single Molecule Imaging in Cells with Near Infra-Red Dyes. PLoS One 2012;7:e36265. https://doi.org/10.1371/journal.pone.0036265.
- [61] Bradley L, Sipocz B, Robitaille T, Tollerud E, Vinícius Z, et al. astropy/photutils: v0.6. Zenodo database 2019. https://10.5281/zenodo.2533376.